Journal of Electronic Research and Application, 2025, Volume 9, Issue 4
http://ojs.bbwpublisher.com/index.php/JERA
ISSN Online: 2208-3510
ISSN Print: 2208-3502

Temporal SU(1,1) Interferometer Based on Four-Wave Mixing Time Lens and Its Applications in Ultrafast Time-Frequency Manipulation

Tianyu Liu, Zepeng Liu*

East China Normal University, Shanghai 200241, China

**Author to whom correspondence should be addressed.*

Abstract: Temporal optics, which enables lossless manipulation of ultrafast pulses, offers a new dimension for the regulation of quantum optical fields. In this paper, we established a temporal Fourier transform (TF) system based on a four-wave mixing (FWM) time lens and constructed a full quantum theoretical model for the resulting temporal SU(1,1) interferometer. This interferometer has high temporal resolution, can impose interference in both time and frequency domains, and is sensitive to the phase derivative. By introducing linear time-varying phase modulation, we achieved sub-picosecond precision in temporal autocorrelation measurements and generated an optical frequency comb with a fixed interval based on a feedback iteration mechanism. Theoretical analysis reveals the crucial regulatory role of time-frequency coupling in quantum interference, providing novel solutions for ultrafast quantum imaging, temporal mode encoding, and the generation of optical frequency quantization.

Keywords: Temporal SU(1,1) interferometer; Four-wave mixing time lens; Optical frequency comb; Temporal optics

Online publication: August 8, 2025

1. Introduction

Temporal optics is an important branch of modern photonics, deriving its theoretical foundation from the mathematical duality between the dispersion effects of narrowband optical pulses and the diffraction phenomena of paraxial light beams [1–3]. This duality establishes a unified framework for describing physical laws in the space-time domain, allowing classical spatial optics theories to be extended to the temporal domain.

In temporal optical systems, temporal imaging has become a key research focus due to its ability to stretch and compress ultrafast waveforms without distortion. Its core component is the time lens, which achieves precise control of optical pulse wavefronts in the time domain [4,5] by introducing quadratic temporal phase modulation (mathematically analogous to the quadratic spatial phase modulation of conventional spatial lenses). Friberg's group developed a theoretical model for temporal ghost imaging based on correlated imaging principles [6]. Genty's

team experimentally demonstrated temporal imaging characteristics of femtosecond pulses in nonlinear media [7]. Kolobov's group established a complete quantum theory of temporal imaging, revealing how vacuum quantum fluctuations limit system resolution [8]. Notably, Jin's research group mapped photon frequency correlations to propagation time and direction correlations through time-space dispersion coupling, achieving long-distance temporal quantum imaging in optical fibers [9]. This work provides new approaches for applying temporal optics in quantum communication systems.

The phase measurement sensitivity of an interferometer determines its precision measurement capability. Classical SU(2) interferometers, using linear beam splitters, have their phase sensitivity limited by the shot noise limit ($1/\sqrt{N}$, where N is the total photon number). In 1986, Yurke *et al.* proposed the SU(1,1) interferometer concept, replacing traditional beam splitters with nonlinear optical devices (such as parametric amplifiers) to achieve phase sensitivity reaching the Heisenberg limit ($1/N$) [10].

However, traditional SU(1,1) interferometers with spatial configurations suffer from limitations including vacuum noise accumulation and modes mismatch. Recent developments in temporal optics have provided new approaches for interferometer design. For instance, temporal SU(1,1) interferometers implement path differences through time delays rather than spatial separation (e.g., utilizing nonlinear effects in optical fibers). Since the optical fields propagate along the same spatial path, losses caused by spatial modes mismatch can be reduced.

Moti Fridman's research group demonstrated a temporal SU(1,1) interferometer using a temporal Fourier transform system as the nonlinear beam splitter and verified its ultrafast phase response characteristics [11]. However, their research primarily focused on experimental observations, and the fundamental quantum dynamics of the system remain not fully understood, particularly the time-frequency coupling mechanism and its role in quantum resource generation.

For conventional time lenses, if the input pulse is too short (i.e., has excessive bandwidth), the excessive dispersion broadening before the time lens may cause the pulse to exceed the finite temporal aperture (available time window) of the time lens [12,13]. This effect severely limits the achievable temporal resolution of the system. FWM is a third-order nonlinear optical effect that enables frequency conversion and phase matching through wave interactions in nonlinear media. Unlike traditional time lenses (typically rely on electro-optic modulation or dispersion compensation), FWM-based phase modulation operates at ultrafast timescales (femtosecond to picosecond). This characteristic potentially allows signal processing within shorter time windows, thereby reducing the requirement for pre-dispersion broadening [14–16].

This paper investigates the application of FWM-based time lenses in SU(1,1) quantum interferometers. We theoretically derive general expressions for the full quantum input-output relations of systems incorporating dispersive media and FWM time lenses, and provide analytical expressions for the temporal intensity distribution of the interferometer's output field. Further research shows that by introducing linear time-varying phase modulation in the Fourier plane, an optical frequency comb structure can be generated at the idler output through a feedback iteration mechanism. The comb spacing is controlled by the modulation parameters. These findings reveal the physical essence of time-frequency domain coupling in temporal nonlinear interference and provide a novel non-mode-locked approach for optical frequency comb generation.

2. Quantum description of the temporal Fourier transform system

The TF system illustrated in **Figure 1(a)** consists of an input dispersive medium, a time lens, and an output dispersive medium. The time lens can be implemented via nonlinear processes; in this work, we adopt FWM

process. This system operates analogously to a spatial 2f system and can perform Fourier transforms on input signals [17–19]. The transformation is achieved by positioning the input and output planes at the focal planes on either side of the time lens, hence referred to as a "temporal 2f system."

In this work, we treat the signal and idler as quantum operators and the pump as a classical field. All optical waves are assumed to be narrowband, with carrier frequencies ω_μ (where μ= {s, i, p} denotes the signal, idler, and pump, respectively). Each wave undergoes dispersion in the medium, characterized by wave vector that is dependent on the frequency ω. Expanding $k_\mu(\omega)$ near $\Omega=\omega-\omega_\mu$ and retaining the first three terms of the Taylor series, we obtain

$$k_\mu(\omega) \approx k_\mu(\omega_\mu) + \beta_\mu^{(1)}\Omega + \beta_\mu^{(2)}\Omega^2/2 \tag{1}$$

where $\beta_\mu^{(1)} = (dk_\mu / d\Omega)_{\omega_\mu}$ is the inverse group velocity, and $\beta_\mu^{(2)} = (d^2k_\mu / d\Omega^2)_{\omega_\mu}$ is the group velocity dispersion (GVD) at the carrier frequency ω_μ.

For a dispersive medium with $\beta_\mu^{(2)} \neq 0$, the frequency-domain operator acquires a phase shift $\hat{a}_\mu^{(1)}(z+l,\tau) = \hat{a}_\mu^{(0)}(z,\tau)\exp(i\beta_\mu^{(2)}\Omega^2 l/2)$ over propagation distance l. In the time domain, this transformation is expressed as:

$$\hat{a}_\mu^{(1)}(z+l,\tau) = \int_{-\infty}^{\infty} G_{in}(\tau-\tau')\hat{a}_\mu^{in}(z,\tau')d\tau' \tag{2}$$

where $G_{in}(\tau) = \frac{1}{\sqrt{-2\pi i D_{in}}} e^{-i\tau^2/2D_{in}}$, with $D_{in} = \beta_\mu^{(2)} l$ being the group delay dispersion (GDD) of the input dispersive medium.

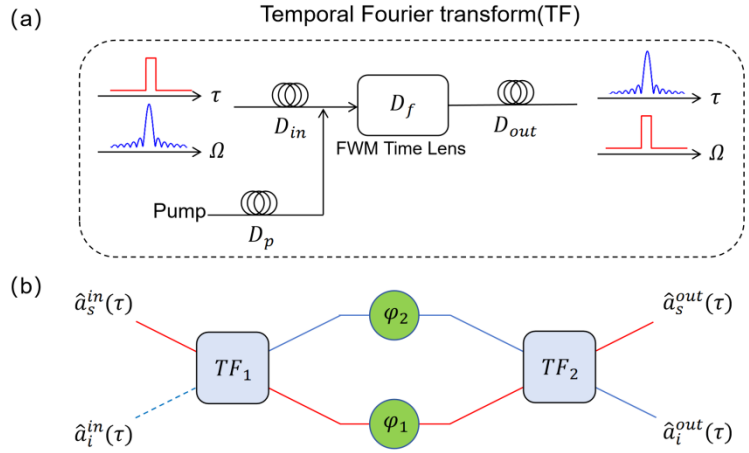

Figure 1. (a) Schematic diagram of TF system. (b) Schematic diagram of the temporal SU(1,1) interferometer. Two TF systems (TF_1 and TF_2) are used as beam splitters.

For perfect phase matching and undepleted pump approximation (the amplitudes and phases of the two classical pump fields are $A_{1,2}$ and $\phi_{1,2}$ respectively), the input-output relations for the FWM time lens can be expressed as:

$$\hat{a}_s^{(2)}(\tau) = G(\tau)a_s^{(1)}(\tau) + ig(\tau)e^{i\phi(\tau)}a_i^{(1)\dagger}(\tau) \tag{3}$$

$$\hat{a}_i^{(2)}(\tau) = ig(\tau)e^{i\phi(\tau)}a_s^{(1)\dagger}(\tau) + G(\tau)a_i^{(1)}(\tau) \tag{4}$$

where $\phi(\tau) = \phi_1(\tau) + \phi_2(\tau)$. Equations (3) and (4) describe the input-output transformation of signal and idler through the time lens, where the coefficients $G(\tau)$ and $g(\tau)$ are given by:

$$G(\tau) = \cosh\left[\eta\chi^{(3)}A_1(\tau)A_2(\tau)L\right] \tag{5}$$

$$g(\tau) = \sinh\left[\eta\chi^{(3)}A_1(\tau)A_2(\tau)L\right] \tag{6}$$

Equations (5) and (6) satisfy the condition $G^2(\tau) - g^2(\tau) = 1$. The optical fields acquire a quadratic phase term $\phi(\tau) = \tau^2 / 2D_f$ from the pump after passing through the time lens, where D_f represents the focal GDD of the time lens, analogous to the focal length of a spatial lens.

Similarly, after passing through the output dispersive medium, whose length is l,

$$\hat{a}_\mu^{(3)}(z+l,\tau) = \int_{-\infty}^{\infty} G_{out}(\tau-\tau')a_\mu^{(2)}(z,\tau')d\tau' \tag{7}$$

where $G_{out}(\tau) = \dfrac{1}{\sqrt{-2\pi i D_{out}}}e^{-i\tau^2/2D_{out}}$, with D_{out} being GDD of the output dispersive medium.

In a TF system based on time-lens utilizing FWM, $-D_{in} = D_{out} = D_f$, and by combining Equations (2), (3), (4), and (7), we derive the general quantized input-output transformation relation of the TF system:

$$\hat{a}_s(\tau) = G(\tau)a_s^{in}(\tau) + g(\tau)\sqrt{\frac{1}{-2\pi i D_f}}\int_{-\infty}^{\infty} a_i^{in\dagger}(\tau')\exp\left(-i\frac{\tau}{D_f}\tau'\right)d\tau' \tag{8}$$

$$\hat{a}_i(\tau) = G(\tau)a_i^{in}(\tau) + g(\tau)\sqrt{\frac{1}{-2\pi i D_f}}\int_{-\infty}^{\infty} a_s^{in\dagger}(\tau')\exp\left(-i\frac{\tau}{D_f}\tau'\right)d\tau' \tag{9}$$

Since the dimension of D_f is $[S^2]$, the above input-output relationship can be expressed as:

$$\hat{a}_{s,i}(\tau) = G(\tau)a_{s,i}^{in}(\tau) + g(\tau)F\{a_{i,s}^{in\dagger}(\tau)\} \tag{10}$$

where $F\{f(\tau)\} = \int_{-\infty}^{\infty} f(\tau')\exp\left(-i\dfrac{\tau}{D_f}\tau'\right)d\tau'$ denotes the time-to-frequency Fourier transform based on $\tau \equiv D_f\Omega$. The above expression is the transformation relation given by Moti Fridman's research group [11].

3. Quantized model of the temporal SU(1,1) interferometer

This section systematically investigates the phase response characteristics of the temporal SU(1,1) interferometer, examining how the time-dependent behavior of additional phases affects quantum interference effects. Based on the temporal properties of phase modulation, the study is categorized into two cases: time-invariant phases and time-varying phases.

3.1. Time-invariant phases

Consider the scheme of a temporal SU(1,1) interferometer shown in **Figure 1(b)**, consisting of two TF systems, with the structure of each TF system illustrated in **Figure 1(a)**. For the initial input state configuration, a coherent state is injected into the signal port, while the idler port remains in a vacuum state. At the Fourier plane after the first TF system, we introduce additional phases denoted as φ_1 and φ_2. These signals are then fed into the second time-frequency system TF_2, which performs an inverse Fourier transform. Under the condition of identical time-lens focal lengths, i.e. $D_{f1} = D_{f2} = D_f$, it is noteworthy that their gains can still differ. The output intensity of the interferometer is given by:

$$I_s(\tau) = [G_1^2 G_2^2 + g_1^2 g_2^2 + 2G_1 G_2 g_1 g_2 \cos(\varphi_1 + \varphi_2)]\left|\alpha(\tau)\right|^2 + 2G_1 G_2 g_1 g_2 \cos(\varphi_1 + \varphi_2) + g_1^2 G_2^2 + G_1^2 g_2^2 \tag{11}$$

$$I_i(\tau) = [g_1^2 G_2^2 + G_1^2 g_2^2 + 2G_1 G_2 g_1 g_2 \cos(\varphi_1 + \varphi_2)]\left|F\{\alpha(\tau)\}\right|^2 + 2G_1 G_2 g_1 g_2 \cos(\varphi_1 + \varphi_2) + g_1^2 G_2^2 + G_1^2 g_2^2 \tag{12}$$

here G_i and g_i are the gain coefficients of the *i–th* time lens, and the complex amplitude $\alpha(\tau)$ characterizes the eigenvalue relation $\hat{a}(\tau)|\alpha\rangle = \alpha(\tau)|\alpha\rangle$ of the annihilation operator $\hat{a}(\tau)$ with respect to the coherent state $|\alpha\rangle$. For the spatial SU(1,1) interferometer, the output intensity expressions are:

$$I_s(\tau) = \left[G_1^2 G_2^2 + g_1^2 g_2^2 - 2G_1 G_2 g_1 g_2 \cos(\varphi_1 + \varphi_2)\right]\left|\alpha(\tau)\right|^2 + g_1^2 G_2^2 + G_1^2 g_2^2 - 2G_1 G_2 g_1 g_2 \cos(\varphi_1 + \varphi_2) \tag{13}$$

$$I_i(t) = \left[g_1^2 G_2^2 + G_1^2 g_2^2 - 2G_1 G_2 g_1 g_2 \cos(\varphi_1 + \varphi_2)\right]\left(\left|\alpha(\tau)\right|^2 + 1\right) \tag{14}$$

Comparative analysis reveals that the temporal and spatial SU(1,1) interferometers exhibit identical output intensity expressions, both demonstrating nonlinear interference characteristics dependent on phase parameters φ_1 and φ_2, manifested as modulation features in the temporal waveform $\alpha(\tau)$. This universality originates from the symmetric design of the time-frequency transformation systems in the interferometer architecture, where the inverse Fourier transform is implemented by the TF_2 module precisely cancels the time-frequency conversion effect of the TF_1 module. The distinctive feature lies in the idler port of the temporal SU(1,1) interferometer, which exhibits signal reconstruction behavior: its output intensity is proportional to the temporal projection of the spectral components of $\alpha(\tau)$ after reconstruction through the time-frequency transformation system. This constitutes the fundamental physical mechanism distinguishing temporal SU(1,1) interferometers from their spatial counterparts. The unique time-frequency entanglement characteristics provide novel manipulation capabilities for quantum precision measurements.

3.2. Time-varying phases

To highlight the temporal characteristics of the temporal SU(1,1) interferometer, we introduce a phase $\varphi_2=\beta_2 + \gamma_2\tau$ which varies linearly with time on the idler at the Fourier plane while leaving the signal unmodulated. The signal and idler are then fed into TF_2, yielding the output optical fields at both ports of the interferometer:

$$\hat{a}_s^{out}(\tau)=G_1G_2a_s^{in}(\tau)+g_1G_2\sqrt{\frac{1}{-2\pi iD_{f1}}}\int a_i^{in\dagger}(\tau')\exp\left(-i\frac{\tau}{D_{f1}}\tau'\right)d\tau' \tag{15}$$
$$+G_1g_2\exp(-i\beta_2)\sqrt{\frac{1}{-2\pi iD_{f2}}}\int \hat{a}_i^{in\dagger}(\tau')\exp\left[-i\left(\frac{\tau}{D_{f2}}+\gamma_2\right)\tau'\right]d\tau'$$
$$+g_1g_2\exp(-i\beta_2)\sqrt{\frac{D_{f1}}{D_{f2}}}\hat{a}_s^{in}\left(\frac{D_{f1}}{D_{f2}}\tau+\gamma_2D_{f1}\right)$$

$$\hat{a}_i^{out}(\tau)=G_1G_2a_i^{in}(\tau)\exp(i\varphi_2)+g_1G_2\exp(i\varphi_2)\sqrt{\frac{1}{-2\pi iD_{f1}}}\int a_s^{in\dagger}(\tau')\exp\left(-i\frac{\tau}{D_{f1}}\tau'\right)d\tau'$$
$$+G_1g_2\sqrt{\frac{1}{-2\pi iD_{f2}}}\int \hat{a}_s^{in\dagger}(\tau')\exp\left(-i\frac{\tau}{D_{f2}}\tau'\right)d\tau'+g_1g_2\sqrt{\frac{D_{f1}}{D_{f2}}}a_i^{in}\left(\frac{D_{f1}}{D_{f2}}\tau\right) \tag{16}$$

here D_{fi} denotes the focal GDD of the *i–th* time lens, where $i=\{1,2\}$. These two equations constitute the fully quantized input-output field theory for the temporal SU(1,1) interferometer. This theoretical framework not only comprehensively characterizes the quantum correlation dynamics between the signal and idler fields, but also reveals the physical origin of quantum-enhanced sensitivity in temporal interferometers: through the FWM process, the two-photon correlation amplification mechanism (G_1G_2 and g_1g_2 terms) compresses input quantum noise into orthogonal quadratures, while the unitarity of the time-frequency transformation ensures nondestructive noise correlation transfer between temporal and spectral domains. By tuning the time-varying phase derivative γ in $\varphi_2=\beta_2+\gamma_2\tau$, it provides a controllable mathematical parameter for ultrafast quantum sensing.

For simplicity, we still consider two time lenses with equal focal lengths and adopt the single-arm coherent-state injection scheme. The output intensities are then:

$$I_s(\tau)=G_1^2G_2^2\left|\alpha(\tau)\right|^2+G_1G_2g_1g_2e^{-i\beta_2}\alpha^*(\tau)\alpha(\tau+\gamma_2D_f) \tag{17}$$
$$+G_1G_2g_1g_2e^{i\beta_2}\alpha(\tau)\alpha^*(\tau+\gamma_2D_f)+g_1^2g_2^2\left|\alpha(\tau+\gamma_2D_f)\right|^2$$
$$+2G_1G_2g_1g_2\cos(\beta_2)+G_1^2g_2^2+g_1^2G_2^2$$

$$I_i(\tau)=\left[g_1^2G_2^2+G_1^2g_2^2+2G_1G_2g_1g_2\cos(\gamma_2\tau+\beta_2)\right]\left|F\{\alpha(\tau)\}\right|^2 \tag{18}$$
$$+2G_1G_2g_1g_2\cos(\gamma_2\tau+\beta_2)+g_1^2G_2^2+G_1^2g_2^2$$

The output intensity of the idler is proportional to the temporal projection of the reconstructed spectral components $\alpha(\omega)$ of $\alpha(\tau)$ through the time-frequency transformation system. This characteristic fundamentally stems from the dual functionality of the time-lens system: implementing Fourier-domain mapping between time and frequency (t→ω) via dispersive media, and facilitating cross-domain transfer of quantum noise correlations through FWM nonlinear processes. Specifically, when the input signal passes through the TF_1 module, its spectral information is encoded into the temporal distribution of the idler. The inverse transformation by the TF_2 module then converts the spectral-phase modulation φ into a temporal displacement γ/ξ, ultimately achieving temporal reconstruction of spectral components at the detector.

This time-frequency coupling effect embodies profound physical significance: first, Nonlocal transfer of quantum noise correlations during time-frequency conversion enables phase-derivative sensitivity to surpass the time-bandwidth product limit of conventional interferometers (e.g., achieving 1/20 rad/ps phase-derivative sensitivity as experimentally demonstrated in reference [11]); second, Linear spectral-to-temporal mapping via time-stretch systems allows simultaneous acquisition of temporal waveforms and spectral features in single-shot measurements, realizing full-field characterization of ultrafast signals (0.5 ps temporal resolution and 0.007 nm spectral resolution in reference [11]). Such unique time-frequency entanglement establishes a novel operational dimension for quantum metrology. For instance, by tuning the EOM frequency, one can actively switch the interferometer's operational mode (temporal-sensitivity/spectral-sensitivity), opening new avenues for ultrafast quantum state tomography and non-equilibrium dynamics studies.

4. Quantum optical frequency comb based on temporal SU(1,1) interferometers

We define $\Delta\tau$ as the temporal width of the input signal $\alpha(\tau)$. In numerical simulations, we use a narrow Gaussian peak with $\Delta\tau$=1ps as the test case. When $\gamma_2 D_f \gg \Delta\tau$, Eq. (17) reduces to Eq. (11), corresponding to the $\gamma_2 D_f < 1ps$ area in Fig. 2(a). However, for $\gamma_2 D_f < \Delta\tau$, the term $\alpha^*(\tau)\alpha(\tau+\gamma_2 D_f)$ vanishes, and the detector no longer registers the self-coupling component of the signal. Instead, a second signal is observed after a time delay $\gamma_2 D_f$, as illustrated in **Figure 2(a)**. This property enables precise measurements of temporal delays and autocorrelation characteristics in signal processing. By tuning the focal length of the time lens, one achieves fine control over signal time delays and accurate measurement of temporal signal widths. The system can also be applied to frequency-resolved optical gating (FROG) for femtosecond pulse phase distortion detection. Unlike conventional FROG setups that rely on motorized translation stages for delay control, the temporal SU(1,1) interferometer's output allows delay tuning at the scale of the signal's temporal width $\Delta\tau$, thereby achieving superior measurement precision.

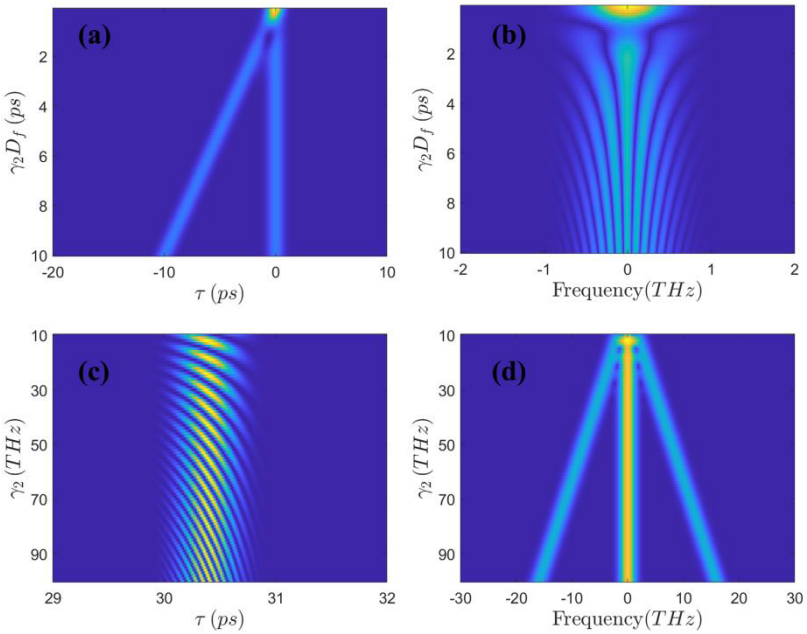

Figure 2. Output intensity pattern of temporal SU(1,1) interferometer. Input is a narrow Gaussian peak with a temporal width of 1 ps. (a)(b) Output signal intensity and its Fourier transform, (c)(d) Output idler intensity and its fourier transform.

For the idler output intensity, γ_2 controls the frequency of interference oscillations. As γ_2 increases, the interference fringes oscillate faster, as shown in **Figure 2(c)**. Applying the Fourier transform to Eq. (18) and invoking the frequency-domain convolution theorem, we obtain:

$$I_i(\Omega) = G_1 G_2 g_1 g_2 e^{i\beta_2} \left[\left| \alpha\left(-D_f\Omega - \gamma_2 D_f\right) \right|^2 + \left| \alpha\left(-D_f\Omega + \gamma_2 D_f\right) \right|^2 \right] + \left(g_1^2 G_2^2 + G_1^2 g_2^2\right) \left| \alpha\left(-D_f\Omega\right) \right|^2 \tag{19}$$

The output idler spectrum splits into a central frequency ω_0 and two sidebands at $\omega_0 \pm \gamma_2$. This property enables the generation of an optical frequency comb with tooth spacing $\gamma_2 D_f$ by cascading multiple temporal SU(1,1) interferometers or by feeding the idler output back into the signal input port. In numerical simulations, a millisecond-scale Gaussian pulse (center wavelength: 1550 nm, spectral width: 1 kHz) was injected into the signal port. After ten feedback iterations, the resulting idler spectral intensity, as shown in **Figure 3**, approximates the comb distribution given by

$$\omega_n = \omega_0 \pm n\gamma_2 D_f \tag{20}$$

here, ω_0 denotes the center frequency of the initial signal light, and $\gamma_2 D_f$ represents the inter-tooth spacing of the frequency comb. The comb tooth at the center frequency exhibits the highest energy, with a gradual decrease on both sides due to nonlinear gain saturation and accumulated phase mismatch. The actual number of comb teeth is limited by the system's gain bandwidth and energy distribution. Even with infinite feedback, the number of comb teeth in this method remains fundamentally limited. Moreover, as the number of iterations increases, the energy becomes progressively more concentrated at the center frequency.

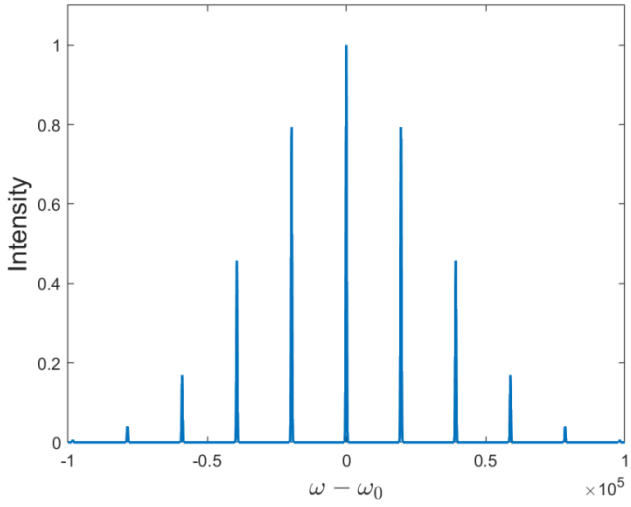

Figure 3. Idler output intensity of the temporal SU(1,1) interferometer after feedback iteration

Compared to existing frequency combs, this comb features significantly narrower inter-tooth spacing at the 10 kHz level. Such narrow bandwidth enables applications in dense wavelength-division multiplexing (DWDM). Conventional DWDM systems typically employ 50 GHz channel spacing, with single-fiber capacities of about 10 Tbps, but face limitations in source stability and spectral resource utilization. This comb can reduce channel

spacing below 12.5 GHz, supporting ultra-dense WDM (UDWDM) [20]. It retains the high signal-to-noise ratio (sharp peak intensity) of existing combs, which reduces bit-error rates, and further pushing channel spacing far below the GHz regime, thereby dramatically increasing fiber capacity.

5. Conclusion

This work establishes a full quantum theoretical framework for a temporal SU(1,1) interferometer based on temporal Fourier-transform systems, revealing their unique advantages in ultrafast time-frequency control and quantum information processing. The study demonstrates that by introducing linear time-varying phase modulation at the Fourier plane, the interferometer achieves temporal autocorrelation measurements at the sub-picosecond scale, with sensitivity significantly surpassing conventional mechanical delay methods (e.g., FROG techniques). Furthermore, through a feedback iteration mechanism, the idler output generates an optical frequency comb with fixed inter-tooth spacing (precisely controlled by phase modulation parameters), providing an efficient solution for quantized optical frequency synthesis. This research not only deepens the physical understanding of temporal nonlinear quantum interference but also lays the theoretical foundation for cutting-edge applications, including ultrafast quantum imaging, temporal-mode encoding, and quantum control of frequency combs.

Disclosure statement

The authors declare no conflict of interest.

References

[1] Tournois P, 1964, Optical Analogy of Pulse Compression. Proceedings of the Academy of Sciences, 258(15): 3839–3842.

[2] Tournois P, Vernet JL, Bienvenu G, 1968, On the Optical Analogy of Certain Electronic Assemblies: Formation of Temporal Images of Electrical Signals. Proceedings of the Academy of Sciences, 267: 375–378.

[3] Akhmanov SA, Sukhorukov AP, Chirkin AS, 1969, Nonstationary Phenomena and Space-Time Analogy in Nonlinear Optics. Soviet Physics - Journal of Experimental and Theoretical Physics, 28(4): 748–757.

[4] Kolner BH, Nazarathy M, 1989, Temporal Imaging with a Time Lens. Optics Letters, 14(12): 630–632.

[5] Kolner BH, 1994, Space-Time Duality and the Theory of Temporal Imaging. IEEE Journal of Quantum Electronics, 30(8): 1951–1963.

[6] Setala T, Shirai T, Friberg AT, 2010, Fractional Fourier Transform in Temporal Ghost Imaging with Classical Light. Physical Review A, 82(4): 043813.

[7] Ryczkowski P, Barbier M, Friberg AT, et al., 2016, Ghost Imaging in the Time Domain. Nature Photonics, 10(3): 167–170.

[8] Patera G, Horoshko DB, Kolobov MI, 2018, Space-Time Duality and Quantum Temporal Imaging. Physical Review A, 98(5): 053815.

[9] Dong S, Zhang W, Huang Y, et al., 2016, Long-Distance Temporal Quantum Ghost Imaging Over Optical Fibers. Scientific Reports, 6(1): 26022.

[10] Yurke B, McCall SL, Klauder JR, 1986, SU(2) and SU (1,1) Interferometers. Physical Review A, 33(6): 4033.

[11] Meir S, Tamir Y, Duadi H, et al., 2023, Ultrafast Temporal SU(1,1) Interferometer. Physical Review Letters, 130(25):

253601.

[12] Bennett CV, Kolner BH, 2002, Aberrations in Temporal Imaging. IEEE Journal of Quantum Electronics, 37(1): 20–32.

[13] Salem R, Foster MA, Gaeta AL, 2013, Application of Space–Time Duality to Ultrahigh-Speed Optical Signal Processing. Advances in Optics and Photonics, 5(3): 274–317.

[14] Shi J, Patera G, Kolobov MI, et al., 2017, Quantum Temporal Imaging by Four-Wave Mixing. Optics Letters, 42(16): 3121–3124.

[15] Kuzucu O, Okawachi Y, Salem R, et al., 2009, Spectral Phase Conjugation Via Temporal Imaging. Optics Express, 17(22): 20605–20614.

[16] Foster MA, Salem R, Okawachi Y, et al., 2009, Ultrafast Waveform Compression Using a Time-Domain Telescope. Nature Photonics, 3(10): 581–585.

[17] Mouradian LK, Louradour F, Messager V, et al., 2000, Spectro-Temporal Imaging of Femtosecond Events. IEEE Journal of Quantum Electronics, 36(7): 795–801.

[18] Foster MA, Salem R, Geraghty DF, et al., 2008, Silicon-Chip-Based Ultrafast Optical Oscilloscope. Nature, 456(7218): 81–84.

[19] Schroder J, Wang F, Clarke A, et al., 2010, Aberration-Free Ultra-Fast Optical Oscilloscope Using a Four-Wave Mixing Based Time-Lens. Optics Communications, 283(12): 2611–2614.

[20] Fortier T, Baumann E, 2020, Author Correction: 20 Years of Developments in Optical Frequency Comb Technology and Applications. Communications Physics, 3(1): 85.